

## MICROSTRUCTURE AND PROPERTIES OF HIGH-STRENGTH MORTAR CURED AT VARIOUS CONDITIONS

H. UCHIKAWA

Kanazawa Institute of Technology, Nonoichi, Ishikawa Prefecture,  
JAPAN

S. HANEHARA and M. UZAWA

Chichibu Onoda Cement Corporation, Central Research Laboratory,  
Sakura, Chiba Prefecture, JAPAN

### Abstract

The relationship between microstructure and properties of high-strength mortar cured at various conditions were investigated using normal portland cement and silica fume cement containing 10% of silica fume. By the steam curing, the strength of SFC was remarkably increased through the acceleration of cement hydration and pozzolanic reaction. The strength of mortar after steam-curing was, however, hardly increased though it was additionally autoclave-cured and oven-cured. The linearity of stress-strain curve of mortar under the loading of compressive strength was much improved by temperature-increasing curing. The static modulus of elasticity of the SFC mortar was lower than of NPC mortar especially in temperature-increasing curing. The reason for these phenomena were discussed in relation to the microstructure-related characters including porosity, pore size distribution, crack of mortar, and kind, crystallinity, quantity and rearrangement of produced hydrates.

Key words: High strength mortar, Steam curing, Autoclave curing, Oven curing, Strength, Stress-Strain curve, Modulus of elasticity, Microstructure

## 1 Introduction

Temperature-increasing curing including steam and autoclave curings is widely used for quickly developing the strength of concrete in the manufacturing process of the concrete products. Reactive powder concrete (RPC) which has recently been developed (Richard et al. 1994) for producing ultra-high strength concrete product is cured at a temperature from 250 to 400°C under normal pressure. Some papers concerning the pore structures of hydrate and hardened mortar formed during the curing have been reported (Dugat et al. 1996, Kalousek 1966). In those papers, however, the mechanical properties including strength and modulus of elasticity and microstructures of the hardened mortar are hardly described.

This paper traces the effects of the mixture proportion of mortar, curing conditions and addition of admixture on the hydration reaction of cement and the composition and formation of microstructure of cement paste, correlates those characters with the compressive strength and stress-strain characteristics of hardened mortar. Based on those data, the relationship between the microstructure of high-strength mortar and its properties were discussed.

## 2 Samples and experimental methods

### 2.1 Preparation of samples and test specimens

Normal portland cement (NPC), silica fume cement (SFC) containing 10% of silica fume and Ogasa sand were used to prepare the test specimens of mortar with the dimensions of 4 × 4 × 16 cm at W/C ratio of 0.25 and S/C of 1.0. Character of these materials are listed in Table 1. Two percent (2.0%) of a naphthalene sulfonic acid-based high-performance water-reducing agent was added to the mixture for keeping the fluidity of fresh mortar. Cylindrical test specimens 10 cm high and 5 cm in diameter were prepared from the same mixture as above for measuring the compressive

Table 1. Character of cement, silica fume and sand

	Chemical composition (%)								Specific surface Area
	SiO <sub>2</sub>	Al <sub>2</sub> O <sub>3</sub>	Fe <sub>2</sub> O <sub>3</sub>	CaO	MgO	SO <sub>3</sub>	Na <sub>2</sub> O	K <sub>2</sub> O	
Normal portland cement (NPC)	21.6	5.3	3.3	64.9	1.1	2.3	0.45	0.35	3,290cm <sup>2</sup> /g*
Silica fume	96.0	0.0	0.4	0.8	-	-	0.21	0.45	18.3 m <sup>2</sup> /g**

\*; Blaine specific surface area \*\*; BET surface area

	Particle size distribution (Residue, %)						Specific gravity (g/cm <sup>3</sup> )
	5mm	2.5mm	1.2mm	0.6mm	0.3mm	0.15mm	
Sand (Ogasa)	0.1	11.2	43.5	65.3	79.2	91.9	2.55

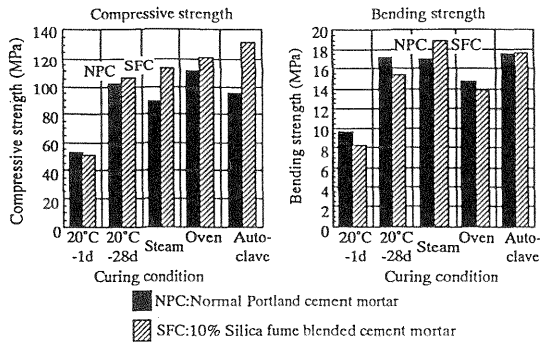


Fig. 1. Strength of hardened mortar cured at various conditons

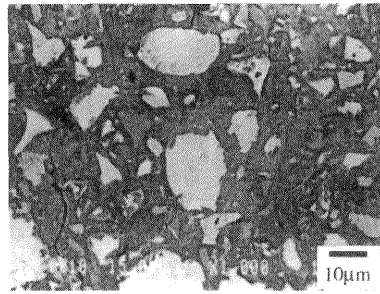


Fig. 2. Cracks generated on the surface of oven cured NPC mortar

effect by the dilution with silica fume.

Although the compressive and bending strengths developed by the steam curing were remarkably improved, those strengths were not so much improved by the oven- and autoclave-curings. Judging from the analytical result of  $\text{Ca}(\text{OH})_2$  shown in Fig. 5, the reason why the strength developed of SFC were higher than those of NPC is considered that the content of calcium silicate hydrate in SFC was increased by the accelerated pozzolanic reaction during the steam curing.

The bending strength of the hardened mortar after the oven curing is lower than that just after the steam curing. Fig. 2 reveals that the size of the test specimen is approximately 5% shrinked by the oven curing, thereby generating a lot of fine cracks on the surface of it. Perhaps the bending strength was decreased by the generation of those cracks on the surface of it.

The ratio of bending strength/compressive strength of SFC was smaller than that of NPC. This suggests that the production of C-S-H or tobermorite by the pozzolanic reaction largely affects the improvement of the compressive strength.

### 3.1.2 Stress-strain characteristics

Fig. 3 illustrates stress-strain curves of hardened mortar under the loading of compressive strength. The figure reveals that the stress-strain curves of hardened mortar prepared by the steam, oven and autoclave curings are almost linear and hardly depend upon the type of cement. The stress-strain curve of a hardened body of uniform material is generally almost linear, while that of uneven composite including concrete and mortar is convex (Swamy 1971). The reason is considered to be as follows.

strength, static modulus of elasticity and strain.

The mortar was released from the mold after cured at 20°C for one day in wet air (briefly “1-day standard curing at 20°C”), then steam-cured at 80°C for three days (briefly “steam curing”) and heat-cured at 250°C for one day in a dryer (briefly “oven curing”) or cured at 180°C under 10 atm for 12 hours in an autoclave (briefly “autoclave curing”). A test specimen was also prepared by water curing at 20°C for 27 days (briefly “28-day standard curing at 20°C”) after releasing the mortar from the mold for comparison.

## **2.2 Experimental methods**

### **2.2.1 Physical property tests**

The strength of hardened mortar was measured according to JIS R-5201. The strain of it was measured by sticking two strain gauges 30 mm long in the center of the side of cylindrical test specimen.

### **2.2.2 Characterization of hardened mortar**

The sample was prepared by cutting cubes with approximately 5 mm of each side out of the hardened mortar with a diamond cutter and immediately dipped into acetone to terminate the hydration and D-dried. The sample for electron probe microanalysis (EPMA) was prepared by grinding the surface of one of them. The samples for the other measurements were prepared by pulverizing them and adjusting the particle size to the specific value. The particle size distribution of the sample for the specific surface area with a scanning BET apparatus was adjusted to 1.0 to 0.5 mm. The hydrate was identified with a rotating cathode type high-power powder X-ray diffractometer. A differential scanning calorimeter was used for determining  $\text{Ca}(\text{OH})_2$ . The pore structure was determined with a mercury-intrusion porosimeter and the microstructure was observed and the composition of it was determined with EPMA. The combined water was measured by the ignition loss test and the insoluble matter was determined according to JIS R-5202.

## **3 Experimental results**

### **3.1 Physical properties of hardened mortar**

#### **3.1.1 Compressive and bending strengths**

The compressive and bending strengths of each sample of hardened mortar are illustrated in Fig. 1. The strengths of SFC at the age within 28 days prepared by the standard curing were equal to or lower than those of NPC, especially the bending strength was conspicuous. Maybe this is because the strength-increasing effect by the increase of the production of C-S-H caused by the pozzolanic reaction does not exceed the strength-decreasing

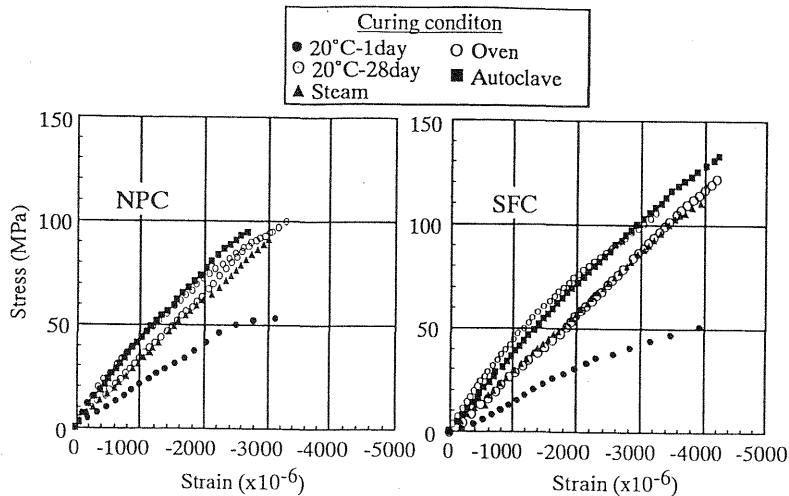


Fig. 3. Stress-strain curve of hardened mortar cured at various conditons

Concrete and mortar have structurally weak transition zones (Uchikawa 1988) on the interface between the aggregate and the cement paste, and the strengths of both materials are different from each other. Stress is, therefore, concentrated into the interface between the aggregate and the cement paste, thereby generating fine cracks and fluctuating the modulus of elasticity (Tanigawa 1976, Hsu et al. 1963, Shah et al. 1966). Since the W/C ratio of the hardened mortar prepared in this study was 0.25, the transition zone hardly existed in it and the structure of hardened mortar (Uchikawa 1997) was uniformalized by the temperature-increasing curing. This may be a reason why the stress-strain curve is almost linear.

To the relationship in concrete between the modulus of elasticity and the compressive strength, the following formula applies (ACI Committee 1984) :

$$E=3,320F^{1/2}+6,900(\text{MPa}) \quad (21<F<83\text{MPa}) \quad (1)$$

where  $E$  = static modulus of elasticity and  $F$  = compressive strength  
 The static modulus of elasticity of concrete in a range of the compressive strength from 21 to 83MPa is determined according to Formula (1). Substituting the values of  $E$  and  $F$  for a formula  $E = F/\epsilon$ , the strain of concrete( $\epsilon$ ) was 950 to 2,200  $\mu\text{m}$ . Determining the strain of the hardened mortar from the limit values of the straight line region of the curve drawn in Fig. 3, the strain of NPC and SFC mortars were 2,800 to 3,200  $\mu\text{m}$  and 3,200 to 4,600  $\mu\text{m}$ , respectively, which were larger than that of concrete.

Meanwhile, the static modulus of elasticity can be determined from the gradient of a straight line connecting the straight line region of the stress-strain curve to the origin. Thus determined values of the static modulus of elasticity are listed in Table 2. The modulus of elasticity of SFC mortar was lower than that of NPC mortar, especially conspicuously lower in the temperature-increasing curing. Maybe this is mainly

Table 2. Static modulus of elasticity of hardened mortar

Curing condition	20°C-1d	20°C-28d	Steam	Oven	Autoclave
NPC	20	40	34	35	40
SFC	15	38	28	29	32

because the contents of highly distortion resistant well-crystallized large-sized crystals including  $\text{Ca(OH)}_2$  and gehlenite hydrate are low.

### 3.2 Composition of hardened mortar

#### 3.2.1 Hydration reaction products

Powder X-ray diffraction profiles of various types of hardened mortar are illustrated in Fig. 4. All of the samples contained ettringite (AFt) and  $\text{Ca(OH)}_2$  and the intensity of diffracted x-ray of AFt had a tendency to slightly decrease in the temperature-increasing curing. That of  $\text{Ca(OH)}_2$  had also a tendency to slightly decrease and a peak considered to be gehlenite hydrate ( $\text{C}_2\text{ASH}_8$ ) was observed at  $2\theta$  of  $17.5^\circ$ . This decreasing tendency of the intensity of diffracted x-ray for  $\text{Ca(OH)}_2$  was conspicuous for SFC mortar. This tendency agrees with the determination result of  $\text{Ca(OH)}_2$  shown in Fig. 5. The decrease in the intensity of diffracted x-ray of  $\text{Ca(OH)}_2$  in the temperature-increasing curing of NPC mortar may be caused by the reaction with the aggregate as mentioned later. That of SFC mortar is considered to be mainly caused by the consumption in the pozzolanic reaction with silica fume.

The existence of C-S-H, xonotlite and tobermorite could not be determined by X-ray diffractometry (XRD). Calcium aluminate sulfate produced by the curing at room temperature is mainly AFm at high W/C ratio, but it is AFt in early age and converted to AFm in later age at low W/C ratio (Uchikawa 1993). The result of this study indicates that the disappearance of AFt and the conversion to AFm at low W/C ratio are hardly accelerated by the temperature-increasing curing.

#### 3.2.2 Content of $\text{Ca(OH)}_2$

The content of  $\text{Ca(OH)}_2$  in the hardened mortar is illustrated in Fig. 5. Although the reduction of  $\text{Ca(OH)}_2$  in SFC mortar was nearly correspond

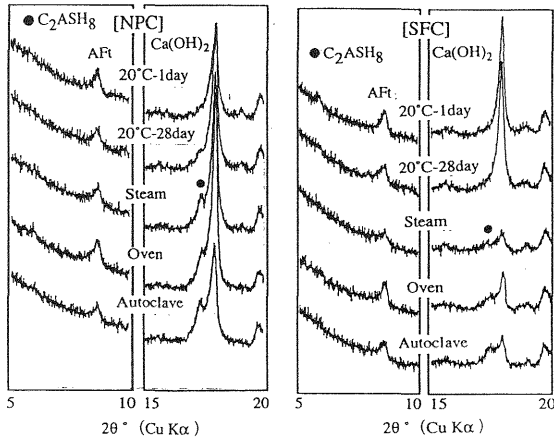


Fig. 4. Powder X-ray diffraction (XRD) profile of hardened mortar cured at various conditions

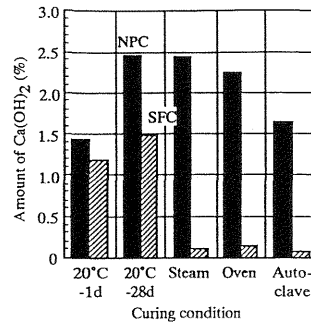


Fig. 5. Amount of  $\text{Ca(OH)}_2$  in hardened mortar cured at various conditions

to the reduction of portland cement by the addition of silica fume in the 1-day curing at  $20^\circ\text{C}$ , there was additional consumption by the pozzolanic reaction of silica fume with  $\text{Ca(OH)}_2$  in the 28-day curing at  $20^\circ\text{C}$ . The consumption of  $\text{Ca(OH)}_2$  by the pozzolanic reaction of silica fume proceeded in a moment in steam curing but it hardly proceeded in the following temperature-increasing curing. The reduction of the content of  $\text{Ca(OH)}_2$  in NPC mortar in the temperature-increasing curing may be caused by the pozzolanic reaction with the aggregate.

### 3.2.3 Content of combined water

Combined water in the hardened mortar measured are illustrated in Fig. 6. The figure reveals that the contents of bound water after both 28-day curing at  $20^\circ\text{C}$  and steam curing and the reaction rates of hydration in both curings are almost the same as each other. Although the content of combined water after the steam curing was hardly changed even by the autoclave curing, it was reduced by the oven curing. Maybe this is because part of the combined water was evaporated by heating it at  $250^\circ\text{C}$ .

### 3.2.4 Content of insoluble residue

The apparent rates of reaction of aggregate (fine sand) and silica fume with  $\text{Ca(OH)}_2$  calculated from insoluble residue measured according to Formula (2) are illustrated in Fig. 7. Assuming that silica fume selectively reacts with  $\text{Ca(OH)}_2$  in SFC, the rate of reaction was calculated. The apparent

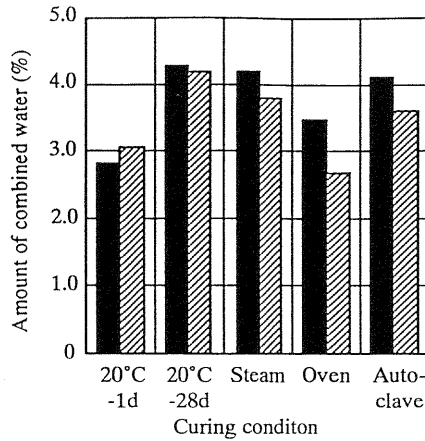


Fig. 6. Amount of combined water of hardened mortar cured at various conditions

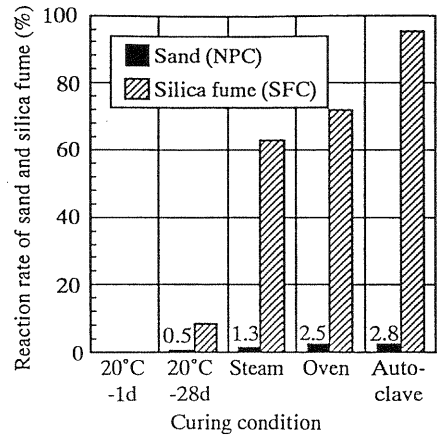


Fig. 7. Reaction rate of sand in NPC mortar and silica fume in SFC mortar

rate of reaction of silica fume was sharply increased by the steam curing and as if reaction were proceeded by the following oven and autoclave curings. On the contrary, the analytical result of the content of  $\text{Ca}(\text{OH})_2$  mentioned before indicated that the content of  $\text{Ca}(\text{OH})_2$  in SFC mortar was hardly changed by the oven and autoclave curings after the steam curing. It is, therefore, considered that the apparent increase of the rate of reaction of silica fume does not correspond to the proceeding of the pozzolanic reaction but to the dissolution of part of silica fume in high-temperature water existing in the atmosphere during the oven and autoclave curings. The reaction of NPC with fine aggregate showed the same tendency as that with silica fume. The rate of reaction was, however, as low as 3% or less.

$$R = (1 - N/M) \times 100 \quad (2)$$

where  $R$  = rate of reaction (%),  $M$  = content of aggregate or silica fume in mortar (mg),  $N$  = content of aggregate or silica fume in insoluble residue (mg).  $N$  was determined by separately measuring the content of insoluble residue in each component.

### 3.2.5 Composition of calcium silicate hydrate

The result obtained by the point analysis of EPMA for the composition of

Table 3. Chemical composition of calcium silicate hydrate in hardened mortar measured by EPMA

Cement	Curing condition	Chemical composition (%)									molar ratio	
		SiO <sub>2</sub>	Al <sub>2</sub> O <sub>3</sub>	Fe <sub>2</sub> O <sub>3</sub>	CaO	MgO	SO <sub>3</sub>	Na <sub>2</sub> O	K <sub>2</sub> O	Total	C/S	C/(S+A)
NPC	20°C -1day	26.4	2.97	1.18	55.3	0.35	2.26	0.19	0.23	88.9	2.25	2.11
	20°C -28day	23.9	3.17	1.58	45.7	0.51	3.34	0.24	0.18	78.6	2.05	1.90
	Steam	25.5	2.83	1.22	45.5	0.32	2.67	0.07	0.05	78.1	1.91	1.79
	Oven	26.2	2.21	1.11	46.0	0.54	3.45	0.20	0.17	79.9	1.88	1.79
SFC	Autoclave	26.9	3.08	1.87	46.7	0.32	2.67	0.07	0.05	81.7	1.86	1.74
	20°C -1day	21.0	3.12	2.40	39.5	0.35	5.20	0.06	0.13	71.8	2.02	1.85
	20°C -28day	31.2	3.28	2.18	43.7	0.33	3.01	0.32	0.23	84.3	1.50	1.41
	Steam	31.2	2.63	0.71	39.9	0.19	2.67	0.31	0.17	77.8	1.37	1.30
	Oven	33.7	2.38	0.64	43.2	0.25	2.44	0.11	0.20	82.9	1.37	1.32
Autoclave	33.4	2.31	0.75	43.5	0.26	1.72	0.11	0.29	82.4	1.40	1.34	

calcium silicate hydrate in the hardened mortar is listed in Table 3. The Ca/Si ratio in calcium silicate hydrate produced was lowered with the proceeding of the hydration, especially the lowering of the Ca/Si ratio in SFC mortar was conspicuous. Although the Ca/Si ratio in calcium silicate hydrate was sharply lowered by the steam curing, it was hardly changed by the following oven and autoclave curings.

### 3.3 Structure of hardened mortar

#### 3.3.1 BET's specific surface area

The specific surface area of the hardened mortar measured by the BET method are illustrated in Fig. 8. Although the BET's specific surface area was increased with the advance of the age and by the steam curing, it was hardly changed by the following autoclave curing but it was sharply decreased by the oven curing. As mentioned later, most of the gel pores once produced were converted to capillary pores 10 to 50 nm in diameter by the oven curing. It is inferred from this that the hardened structure was broken when C-S-H or tobermorite was converted to well-crystallized calcium silicate hydrate including xonotlite, whereupon the BET's specific surface area was reduced.

#### 3.3.2 Pore structure

The pore size distribution in the hardened mortar is illustrated in Fig. 9. The total pore volume decreased and the pore size distribution shifted to the small diameter side with the progress of curing except the oven curing. The total pore volume in the steam curing was larger than that in the 28-day curing at 20°C but the pore size distribution in steam curing was shifted to the small diameter side. The total pore volume was not reduced even by the autoclave curing after the steam curing, but it was increased by the increase of the pores 6 to 50 nm in diameter. Although the pore

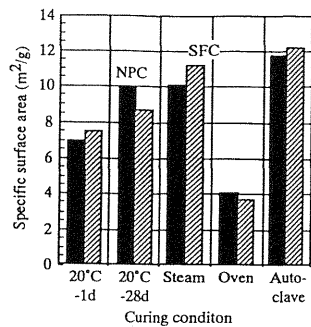


Fig.8. BET specific surface area of hardened mortar cured at various conditions

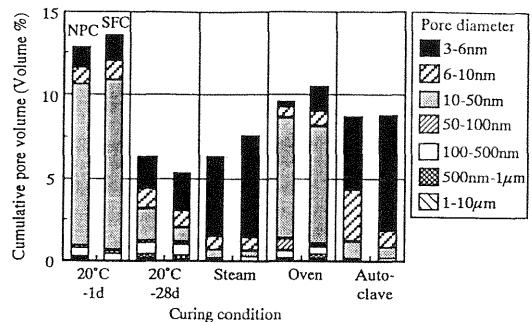


Fig. 9. Pore volume of hardened mortar cured at various conditions

diameter in the SFC mortar was reduced more than that in the NPC mortar by the temperature-increasing curing, the total pore volume was increased. The pores 10 to 50 nm in diameter was more remarkably increased and total pore volume was increased by the oven curing than that after the steam curing. Maybe this is because the hardened structure was changed by the formation of new pores by dehydration and the changes of size, shape, crystallinity and structure of the hydration products by the temperature increase. The decrease of the pores 3 to 6 nm in diameter and the increase of the pores 10 to 50 nm in diameter agree with the measurements of the BET's specific surface area mentioned before.

The changes of the pore volume by the curing after the 1-day curing at 20°C and steam curing used as the basis are illustrated in Fig. 10.

The pores 10 to 100 nm in diameter after the 1-day curing as the basis at 20°C were decreased by the 28-day curing at 20°C and the pores 30 nm in diameter showed the maximum decrease. The pores 10 to 100 nm in diameter were also largely decreased by successive steam curing similar to that in the case of 28-day curing at 20°C and the pores 3 to 10 nm in diameter were increased showing maximum at 4 nm in diameter. This suggests that the calcium silicate hydrate is increased and the produced quantities of calcium silicate hydrate by the steam curing in the NPC and SFC mortars are nearly equal to each other.

The gel pores approximately 3 nm in diameter after the steam curing as the basis were decreased by the oven curing and the capillary pores with 60 and 30 nm in diameter as the central figure in the NPC and SFC mortars, respectively, were increased. Meanwhile, the volume of small diameter

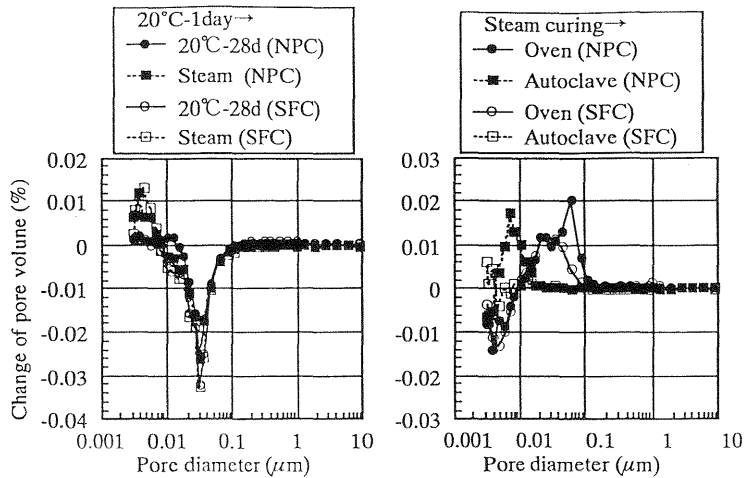


Fig. 10. Difference of pore volume of hardened mortar between cured at 20°C-1day and under steam, and added curing under various conditions

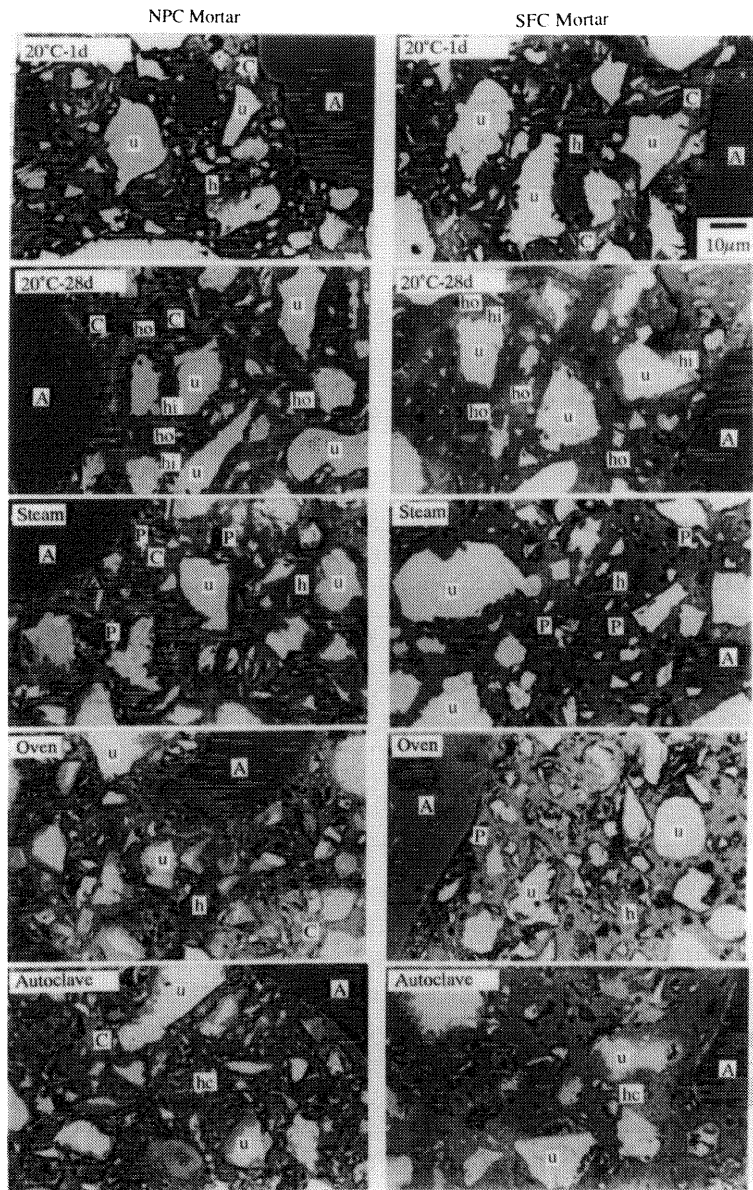
pores in the NPC mortar was remarkably increased by the autoclave curing and that of 6 nm in diameter showed the maximum increase. There was little difference in the SFC mortar before and after autoclave curing.

### 3.3.3 Microstructure

The back scattered electron images of the polished surface of hardened mortar are illustrated in Fig. 11. The thickness of the inner-hydrate layers around unhydrated cement particles was increased with the advance of the ages of both NPC and SFC mortars in the standard curing and the gaps between the unhydrated cement particles were filled with the outer-hydrate. Thus the hardened structure was being densified. Large-sized crystals of  $\text{Ca}(\text{OH})_2$  were observed in the vicinity of the interfaces between cement paste and aggregate in NPC mortar. The densest structure was produced by the 28-day curing at 20°C compared with other curings.

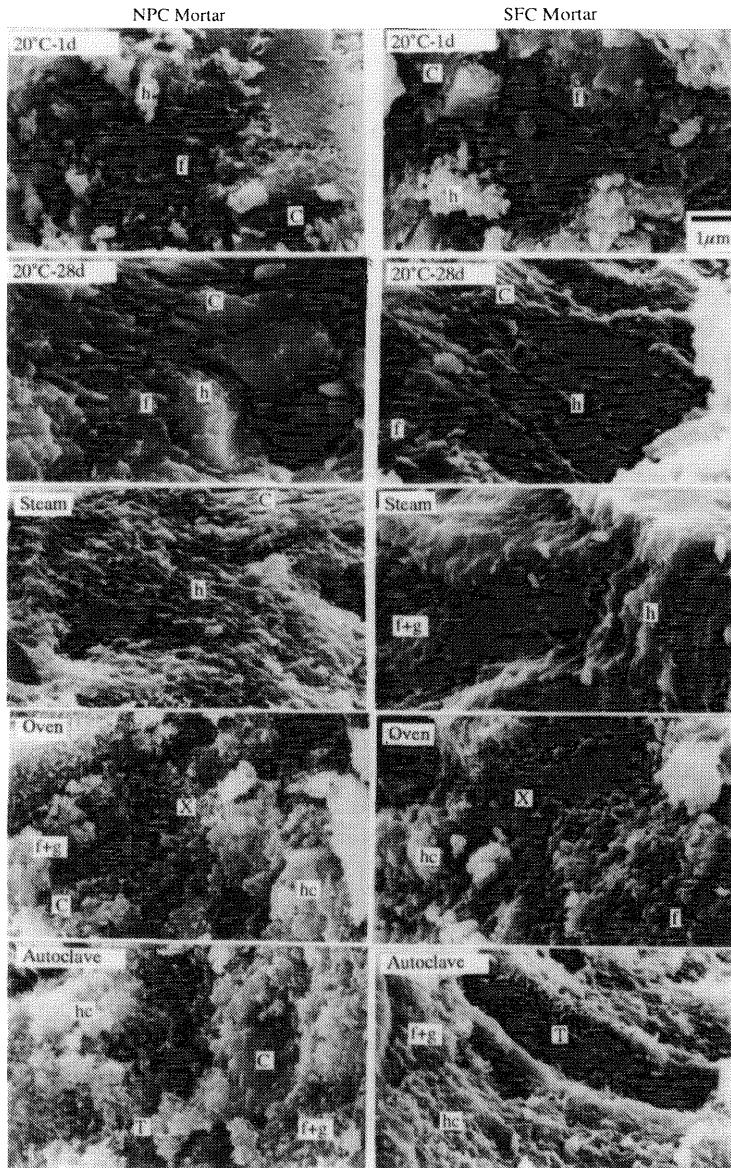
Spherical and ellipsoidal pores of one to several microns were formed in the hardened structure by the steam curing and the volume of them were increased by the oven and autoclave curings. Pores between the interfaces of aggregate and the cement particles considered to be caused by dehydration were slightly increased by the oven curing.

The secondary electron images of a fracture surface of hardened mortar are illustrated in Fig. 12. In the standard curing, the densified hardened structure was observed at the age of 28 days. A lot of large-sized platy



u: Unhydrated cement particle  
 hi:C-S-H Inner hydrate ho:C-S-H Outer hydrate  
 P: Pore hc: Calcium silicate hydrate  
 A: Aggregate h: C-S-H C: Ca(OH)<sub>2</sub>

Fig. 11. Back-scattered electron image of polished surface of hardened mortar cured at various conditions



X: Calcium silicate hydrate(Xonotlite)  
T: Calcium silicate hydrate(Tobermorite)  
hc: Calcium silicate hydrate g: Gehlenite hydrate  
A: Aggregate h: C-S-H C: Ca(OH)<sub>2</sub> f: AFt

Fig. 12. Secondary electron image of fracture surface of hardened mortar cured at various conditions

crystals of  $\text{Ca}(\text{OH})_2$ , platy crystals of AFt and C-S-H filling the gaps between them were observed in the NPC mortar, while a few small-sized crystals of  $\text{Ca}(\text{OH})_2$  and a lot of C-S-H were observed in the SFC mortar. In the steam curing, aggregated structures of calcium silicate hydrate considered to be grown from the C-S-H crystals were observed in the NPC mortar. The hardened structure in the SFC mortar was not so much different from that produced by the 28-day curing at  $20^\circ\text{C}$ . The hardened structure produced by the oven curing was more porous than that produced by the steam curing. This suggests that the hardened structure produced by the steam curing was changed by dehydration of it. Aggregated structures of well-crystallized calcium silicate hydrate which may be xonotlite and those of small-sized platy crystals which may be gehlenite hydrate were also observed in that structure. Although structures similar to the structures produced by the oven curing were observed in the autoclave curing, the size of hydrate was generally smaller and the morphology of crystalline calcium silicate hydrate, which seems to be tobermorite, was slightly different from those produced by the oven curing.

#### **4 Relationship in hardened mortar between structure and physical properties**

##### **4.1 Strength and static modulus of elasticity**

The relationship in the hardened mortar between the strength and static modulus of elasticity and a curve representing Formula (1) are illustrated in Fig. 13. Estrangement of the plots from the curve were large in the mortar after the 1-day curing at  $20^\circ\text{C}$  and in the SFC mortar after the steam, oven and autoclave curings. This is because the maturity of hardened structure produced by the 1-day curing at  $20^\circ\text{C}$  is low and porous and the hydrate is not sufficiently crystallized. The structure of SFC mortar produced by the temperature-increasing curing may also be easily deformable by the stress because the consumption of  $\text{Ca}(\text{OH})_2$  crystal playing a role of the skeleton of the hydrated structure and the production of low-stiffness low-C/S ratio calcium silicate hydrate and of small particle hydrates.

##### **4.2 Relationship between pore volume and compressive strength**

The relationship in the hardened mortar between the total pore volume and the compressive strength is illustrated in Fig. 14. The compressive strength of the mortar produced by the temperature-increasing curing was higher than that produced by the standard curing when pore volume was same and the difference of compressive strength was increased with the increase of the curing temperature. It is known that the compressive

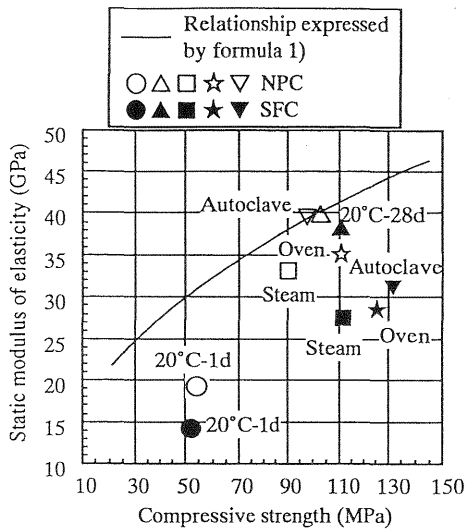


Fig. 13. Relationship between compressive strength and static modulus of elasticity

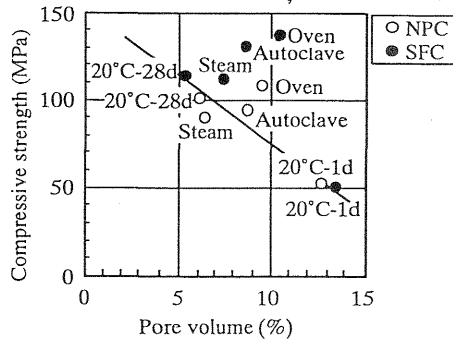


Fig. 14. Relationship between compressive strength and total pore volume

strength depends upon the content of crystalline materials in the hardened mortar as well as the porosity (Crennan et al. 1977). The result of this study agrees well with the previous work.

#### 4.3. Relationship between microstructure and fracture

Applying compressive strength to a uneven composite materials containing pores including mortar and concrete, stress is concentrated into the points with peculiar shape around the pores in it and weak materials, thereby generating and propagating cracks resulting in fracture of the composite. Even applying a load smaller than the fracture stress to that, the hardened structure is changed in such a manner as peeling and breaking of hydrate and formation of large pores by linking small pores to each other when the applied stress exceeds the 60% of fracture stress (Uchikawa et al. 1977). The propagating velocity of cracks depends upon the denseness of hardened structure in such a manner that the propagating velocity of cracks is lowered with the increase of denseness of hardened mortar, so the growth to large cracks is retarded (Uchikawa et al. 1977).

### 5 Summary and conclusions

Normal portland cement mortar and silica fume cement containing 10% of

silica fume mortar prepared at the W/C ratio of 0.25 and the S/C ratio of 1.0 were cured under various conditions. And the effects of the curing conditions and the addition of mineral admixture on the hydration reaction of cement and the formation of micro-structure of hardened mortar, the relationships in the hardened mortar of the composition and structure with the physical properties and the relationship between the microstructure and the fracture process were investigated.

The conclusions obtained in the study are summarized as follows:

- 1) The strength of SFC mortar cured under standard condition was lower than that of NPC mortar within the age of 28 days. Maybe this is because the dilution effect by the addition of silica fume exceeds the effect of the increasing production of C-S-H by the pozzolanic reaction.
- 2) The hydration reaction of cement was accelerated by the steam curing. The strength of SFC mortar was sharply improved by the steam curing through the increase of the production of calcium silicate hydrate with the proceeding of pozzolanic reaction, exceeding the strength of NPC mortar.
- 3) The strength of mortar after the steam curing was hardly increased though it was further autoclave-cured. Even if it was additionally oven-cured, the bending strength was sharply lowered though the compressive strength was slightly improved. The strength of mortar is generally negatively affected by the increase of the volume of pores, the increase of pore diameter and the generation of fine cracks, while it is positively affected by the increase of content of hydrate and the desirable degree of crystallinity of hydrate. It is considered that the compressive strength of oven-cured mortar is affected largely by the latter more than the former, while the bending strength is affected by the former, especially by the generation of fine cracks.
- 4) The volume of pores was increased and the pore size distribution shifted to the large diameter side in the oven-cured mortar. This may be brought by the generation of fine crack caused by the rearrangement of hardened structure by the conversion of tobermorite and others to well-crystallized calcium silicate hydrate including xonotlite by dehydration accompanied with the increase of curing temperature.
- 5) The strength of mortar was higher by the temperature-increasing curing than by the standard curing when the total pore volume is same. This suggests that the compressive strength is largely affected by the content of crystalline materials in the mortar, especially by the degree of crystallinity of calcium silicate hydrate as well as the porosity.
- 6) The stress-strain curve of the mortar under the loading of compressive strength was made more linear by the temperature-increasing curing. Maybe this is because the homogeneity of the hardened structure is improved by the temperature-increasing curing, whereupon the concentration of stress is alleviated.

7)The static modulus of elasticity determined from the gradient of the stress-strain curve of the SFC mortar was lower than that of the NPC mortar. This tendency was conspicuous in the temperature-increasing curing. This is mainly because highly distortion-resistant, well-crystallized large-sized  $\text{Ca}(\text{OH})_2$  crystals are remarkably reduced and the content of well-crystallized gehlenite hydrate crystal is low.

## References

- ACI Committee 363 (1984) State-of-the-Art Report on High-Strength Concrete, **J. of ACI**, 81, 364-411.
- Crennan, J.M., El-Hemaly, S.A.S. and Taylor, H.F.W. (1977) Autoclaved Lime-Quartz Materials I. Some Factors Influencing Strength, **Cem. and Concr. Res.**, 7, 493-502
- Dugat, J., Roux, N. and Bernier, G. (1996) Mechanical Properties of Reactive Powder Concretes, **Material and Structure**, 29, 233-240.
- Hsu, T.T.C., Slate, F.O., Struman, G.M. and Winter, G. (1963) Microcracking of Plane Concrete and the Shape of the Stress-Strain Curve, **J. of ACI**, 60, 209-223.
- Kalousek, G.L. (1966) Autoclave Curing of Concrete in Soviet Union and United State, **J. of ACI**, 63, 817-832.
- Richard, P. and Cheyrezy, M.H. (1994) Reactive Powder Concrete with High Ductility and 200-800MPa Compressive Strength. **Concrete Technology**, SP144-24, 507-517.
- Shah, S.P. and Winter, G. (1966) Inelastic Behavior and Fracture of Concrete, **J. of ACI**, 63, 925-930.
- Swamy, R.N. (1971) Fracture Phenomena of Hardened Paste, Mortar and Concrete, **Proceeding of the International Conference on Mechanical Behavior of Materials**, Kyoto Japan, 132-142.
- Tanigawa, Y. (1976) Model Analysis of Fracture and Failure of Concrete as a Composite Material, **Cem. and Concr. Res.**, 6, 679-690
- Uchikawa, H. Hanehara, S. and Hirao, H. (1977) Influence of Microstructural Change under Stress on the Strength-Related Properties of Hardened Cement Mortar and Paste, **Advanced Cement Based Materials**, 6 [3/4], 87-98

- Uchikawa, H. (1988) Similarities and Discrepancies of Hardened Cement Paste, Mortar and Concrete from the Standpoints of Composition and Structure, **Proceedings of Engineering Foundation Conference 'Advances in Cement Manufacture and Use'** Potosi, Missouri, 1, 271-294.
- Uchikawa, H. (1993) Characterization and Material Design of High-Strength Concrete with Superior Workability, **Proceeding of Cement Technology Symposium, PAC RIM Ceramic Meeting**, Honolulu, Hawaii, Ceramic Transactions, 40, 143-186
- Uchikawa, H. (1997) Role and Regulation of the Transition Zone in Realizing High Performance Concrete, **Proceedings of Third CANMET/ACI International Conference on 'Advances in Concrete Technology'**, Auckland, New Zealand, 109-129